Water Science & Technology

Water Science & Technology Vol 87 No 3, 571 doi: 10.2166/wst.2023.011

Adsorptive removal of Cr(III)–EDTA chelate from an aqueous solution by magnetic mesoporous silica microspheres

Jiahong Wang[a,b,*], Sili Lei[a,b], Tongtong Sun[a,b] and Peiling Han[a,b]

[a] School of Environmental Science and Engineering, Shaanxi University of Science & Technology, Xi'an 710021, China
[b] Shaanxi Key Laboratory of Green Preparation and Functionalization of Inorganic Materials, Xi'an 710021, China
*Corresponding author. E-mail: wangjiahong@sust.edu.cn

ABSTRACT

The 3-aminopropyltrimethoxysilane-modified magnetic mesoporous adsorbent (FNMs/APTES) was synthesized and applied to remove Cr(III)–EDTA chelates from water. The characterization of FNMs/APTES showed that the prepared adsorbent with a magnetic mesoporous structure was successfully grafted by APTES, which has good stability under acid conditions. The maximum capacities of FNMs/APTES for Cr(III)–EDTA adsorption at 15, 25 and 35 °C and pH 4.0 were 12.58, 13.13 and 14.00 $mg \cdot g^{-1}$, respectively. The adsorption isotherm of FNMs/APTES for Cr(III)–EDTA conforms to the Freundlich model, and the adsorption kinetic model accords with the pseudo-second-order kinetic model. Adsorption of Cr(III)–EDTA on the adsorbent was not affected in the presence of Na^+, K^+ and Ca^{2+} even at 100 $mmol \cdot L^{-1}$. Cr(III)–EDTA was anchored on FNMs/APTES through electrostatic interaction between protonated amino groups of adsorbents and Cr(III)–EDTA anions, and Cr(III)–EDTA chelates were adsorbed as a whole on the adsorbent. The Cr(III)–EDTA-saturated adsorbent can be readily regenerated in HCl solution and 83.03% of the initial Cr(III)–EDTA adsorption capacity remains after four adsorption–regeneration experiment cycles. The results highlighted that the FNMs/APTES as a potential adsorbent can be applied for the minimization of Cr(III)–EDTA chelates from water.

Key words: adsorption, amino group-modified magnetic mesoporous silica, Cr(III)–EDTA, regeneration

HIGHLIGHTS

- FNMs/APTES were synthesized and applied to remove Cr(III)–EDTA from water.
- FNMs/APTES exhibits high adsorption capacities for Cr(III)–EDTA.
- Cr(III)–EDTA adsorption was not affected by the presence of high salt ions.
- Cr(III)–EDTA as a whole was combined on the adsorbent by electrostatic interaction.
- Cr(III)–EDTA-saturated adsorbent can be easily regenerated in an acid solution.

GRAPHICAL ABSTRACT

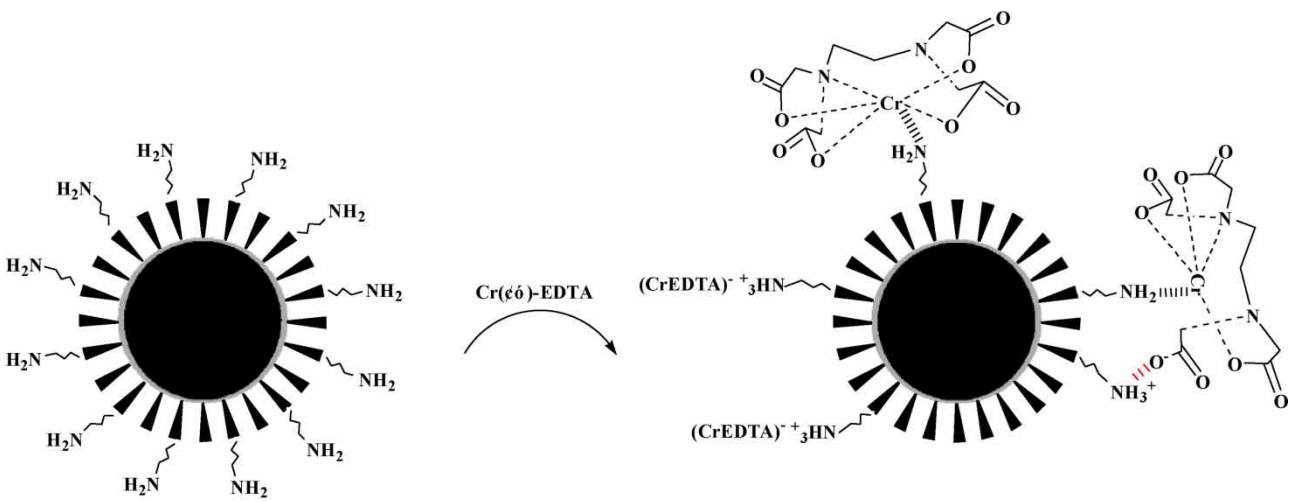

1. INTRODUCTION

Chromium (Cr) pollution of the aquatic environment is widely perceived as an environmental problem due to its nonbiodegradability and toxicity properties (Guan *et al.* 2017; Hai *et al.* 2020). The worldwide use of Cr in many industries, such as electroplating, tannery, metallurgy and organic chemical synthesis, has received great concerns because of its potential threats to environmental safety (Egodawatte *et al.* 2015; Guimaraes *et al.* 2020). In the environment, chromium was mainly in the form of trivalent chromium (Cr(III)) and hexavalent chromium (Cr(VI)). The toxicity and essentiality of Cr depend on its oxidation state (Novotnik *et al.* 2016). Many studies have shown that the excess accumulation of Cr(III) in humans can decrease immune system activity (Wang *et al.* 2019). Furthermore, Cr(III) could be converted into more toxic Cr(VI) during the changes in Eh and pH states (Luther *et al.* 2013; Su *et al.* 2016), which improves the toxicity of Cr(III). Thus, the elimination of Cr(III) ions from water is critical (Eyvazi *et al.* 2019).

For the real-water environment, the dissolved chromium mainly exists in the form of free hydrated ions or complexes (with inorganic or organic ligands). For example, a variety of organic pollutants was found in tannery effluent, which would react with Cr(III) and form diverse Cr(III)-bearing complexes (Chen & Pan 2020). Ethylenediamine tetraacetate (EDTA) is a commonly used chelating agent in industrial production. A stable complex (Cr(III)–EDTA) can be formed by chelation between Cr(III) and EDTA (Novotnik *et al.* 2016). Unlike free hydrated Cr(III), Cr(III)–EDTA is usually stubborn to a traditional treatment method due to its high chemical stability. Therefore, a variety of treatment technologies including chemical precipitation (Lofrano *et al.* 2013; Tang *et al.* 2020), membrane separation (Zhang *et al.* 2021), adsorption (Wang *et al.* 2020a), biological treatment (Xu *et al.* 2022), Fenton-like process (Ye *et al.* 2018), electrochemical reduction (Durante *et al.* 2011) have been employed for the elimination of Cr(III)–chelate. Among these techniques, adsorption has been deemed one of the most promising strategies for removing low concentration of Cr(III) due to its high cost-effectiveness, simple implementation and high efficiency (Liu 2021; Zhang *et al.* 2022).

Recently, many studies have been conducted to remove Cr(III) from water using different adsorbents. For example, montmorillonite-based porous adsorbents were prepared by the gel casting method for the removal of chromium citrate in low concentration (10 mg L^{-1}) in tanning wastewater (Hao *et al.* 2021). DETA-functionalized magnetic carbon adsorbent was found to efficiently remove Cr(III)–EDTA in aqueous solution, and the introduced amino active sites contribute to the improved Cr(III)–EDTA adsorption performance (Wang *et al.* 2021). Note that mesoporous adsorbents were found to be active for heavy metal adsorption even in high-salinity wastewater, for example, EDTA- or DTPA-modified magnetic mesoporous microspheres have a good adsorption performance on Cr(III) in high-salinity organic wastewater (Wang *et al.* 2020a, 2020b, 2020c). While adsorption of heavy metals on mesoporous silica adsorbents is very limited, surface modification with active groups such as amino groups, carboxyl groups and so on, may improve the heavy metal adsorption on mesoporous silica adsorbents. The amino group-modified adsorbents exhibit good adsorption for Cr(III)–EDTA (Wang *et al.* 2020a, 2021). Therefore, amino group-modified mesoporous adsorbent may improve the adsorption efficiency for Cr(III)–EDTA chelate in high-salinity water. Magnetic mesoporous silicon microspheres with large surface areas ordered mesoporous structure and easy modification have attracted much attention for the minimization of organic and inorganic pollutants in water. (3-Aminopropyl) trimethoxy silane (APTES) has a high content of nitrogen atoms, which can provide a large number of available adsorption sites. Therefore, in this study, APTES-modified magnetic mesoporous microspheres (FNMs/APTES) were synthesized to remove Cr(III)–EDTA from wastewater. The kinetics, adsorption equilibrium and effect of water chemical conditions are conducted, and related adsorption mechanism was also advised.

2. MATERIALS AND METHODS

2.1. Reagents and equipment

The chemicals used in this study, $FeCl_3{\cdot}6H_2O$, $NH_3{\cdot}H_2O$, NH_4NO_3, CH_3COONa, ethylene glycol, toluene, tetraethoxysilane (TEOS), hexadecyl trimethyl ammonium bromide (CTAB) were of analytical reagent grade and were purchased from Tianjin Kameiou Chemical Reagent Co., Ltd. (Tianjin City, China). (3-Aminopropyl) trimethoxy silane (APTES) was obtained from Alighting reagent (Shanghai) Co., Ltd. (Shanghai, China).

The morphology of the material was characterized by JEM2100f transmission electron microscope (TEM). D/max2200PC X-ray diffraction (XRD) of Rigaku Company in Japan was used to analyze the crystal structure before and after modification of the material, Cu-K radiation, graphite monochromator, tube voltage of 40 kV, tube current of 30 mA, scanning range of $2\theta = 1$–$70°$. A Nexus 870 Fourier Transform infrared spectrometer (FT-IR) from Nicolet was used to characterize the

adsorbents. The thermogravimetry (TGA) Q500 of TA Company was used to analyze the thermal stability of prepared materials. The ASAP 2460 automatic specific surface area and porosity analyzer was used to characterize the adsorbents' specific surface area and pore size distribution. The elemental distribution and surface chemical composition were analyzed with VG ESCALB MK-II X-ray photoelectron spectrometer (XPS).

2.2. Preparation of FNMs/APTES

The preparation of Fe_3O_4@nSiO_2@mSiO_2 (FNMs) is based on our previous studies (Wang *et al.* 2020c). The Fe_3O_4@nSiO_2@mSiO_2 was modified sequentially with APTES to introduce amine groups. Briefly, 1 g of FNMs was dispersed into 50 mL of anhydrous toluene, and 1 mL of APTES with N_2 atmosphere was added and stirred in an oil bath at 110 °C for 12 h. In the end, the products were magnetically separated, cleaned with toluene and ethanol for several times, and vacuum dried at 60 °C (FNMs/APTES).

2.3. Adsorption of Cr(III)–EDTA by FNMs/APTES

2.3.1. Stability experiment

Typically, 20 mg of FNMs/APTES was dispersed in 50 mL of HCl solution with different concentrations. The concentration of Fe was detected by ICP-OES and the Fe dissolution rate was calculated at different sampling times.

2.3.2. Adsorption experiments

In this study, Cr(III)–EDTA was used to simulate the complex form of Cr(III) in actual wastewater. EDTA–2Na and $Cr(SO_4)_3{\cdot}6H_2O$ were mixed at 2:1 (molar ratio) and stirred at 25 °C for 24 h. All experiments were conducted at pH 4.0. 20 mg of FNMs/APTES was added to 50 mL solution of Cr(III)–EDTA with different initial concentrations (2.5–20 $mg{\cdot}L^{-1}$) at 15, 25 and 35 °C with 140 r min^{-1} for 12 h, respectively. For kinetic study, 200 mg of FNMs/APTES was added to 500 mL of 15 $mg{\cdot}L^{-1}$ of Cr(III)–EDTA solution, sampling at different intervals. Furthermore, the residual Cr(III) concentration of the filtrate was analyzed by ICP-AES after the suspension was filtered by 0.45-μm fiber membrane, and the equilibrium adsorption amount at different temperatures was calculated by Formula (1).

To explore the recycling effect of FNMs/APTES, 0.05 $mol{\cdot}L^{-1}$ HCl solution was used as a desorption agent for the regeneration of Cr(III)–EDTA-saturated FNMs/APTES. After adsorption of Cr(III)–EDTA, the material was added to 200 mL of 0.05 $mol{\cdot}L^{-1}$ HCl solution and stirred for 8 h and then dried. The regeneration experiments were repeated four times.

$$q_e = \frac{(C_0 - C_e)V}{M} \tag{1}$$

where C_0 ($mg{\cdot}L^{-1}$) and C_e ($mg{\cdot}L^{-1}$) are the initial and equilibrium concentrations of Cr(III)–EDTA in solution, respectively. M (mg) is the mass of the adsorbent and V (mL) is the volume of solution.

2.4. Experimental data models

To further explore the adsorption behavior of the FNMs/APTES, Langmuir and Freundlich adsorption isotherm equations were used to fit the experimental data. The linear expression of the Langmuir isotherm is as follows:

$$\frac{C_e}{q_e} = \frac{1}{bq_m} + \frac{C_e}{q_m} \tag{2}$$

The Freundlich model are as follows:

$$lnq_e = lgK_f + \frac{1}{n} lnC_e \tag{3}$$

where q_e ($mg{\cdot}g^{-1}$) is the equilibrium adsorption amount of Cr(III), C_e ($mg{\cdot}L^{-1}$) is the equilibrium concentration of Cr(III), K_f and n are the characteristic constants of Freundlich, q_m ($mg{\cdot}g^{-1}$) is the maximum adsorption capacity of Cr(III)–EDTA and b ($L{\cdot}mg^{-1}$) is the affinity coefficient.

The Gibbs–Helmholtz equation calculated thermodynamic parameters of FNMs/APTES to Cr(III)–EDTA, and analyzed the thermodynamic behavior during the adsorption process. The Gibbs–Helmholtz equation is obtained by the following

equations:

$$\Delta G^{\ominus} = \Delta H^{\ominus} - T\Delta S^{\ominus} \tag{4}$$

$$ln\frac{q_e}{C_e} = \frac{\Delta S^{\ominus}}{R} - \frac{\Delta H^{\ominus}}{RT} \tag{5}$$

where R (8.314 J·mol^{-1}·K^{-1}) is the molar gas constant, T (K) is the temperature, $\Delta H°$ (kJ·mol^{-1}), $\Delta S°$ (J·mol^{-1}·K^{-1}) and $\Delta G°$ (kJ·mol^{-1}) are enthalpy, entropy and Gibbs free energy, respectively.

To study the adsorption rate of Cr(III)–EDTA by FNMs/APTES, the adsorption kinetic models (pseudo-first-order kinetic model and pseudo-second-order kinetic model) were used to simulate the experimental data.

The first-order kinetic model can be expressed as:

$$ln(q_e - q_t) = ln\, q_e - k_1 t \tag{6}$$

The second-order kinetic model can be expressed as:

$$\frac{t}{q_t} = \frac{1}{k_2 q_e^2} + \frac{t}{q_e} \tag{7}$$

where q_e and q_t (mg·g^{-1}) were the equilibrium adsorption capacities, and the adsorption amount at time t (min), k_1 (g·mg^{-1}·min^{-1}) and k_2 (g·mg^{-1}·min^{-1}) represent the rate constants of two kinetic models, respectively.

3. RESULTS AND DISCUSSION

3.1. Characterization of the adsorbents

The TEM images of the FNMs are shown in Figure 1(a) and 1(b). It was observed that the FNMs had identical, clear core–shell structures and monodisperse sphere-shaped particles (Elmobarak & Almomani 2021). The inner part of the microsphere is Fe_3O_4, whereas the outer ring is the coated SiO_2 layer, and the reflecting shell of SiO_2 was to protect the Fe_3O_4 cores under water environment. The SiO_2 layer formed vertical regular holes, which explains the formation of the mesoporous structure (Cheng *et al.* 2017). Meanwhile, as can be seen from the illustration vignette in Figure 1(a), FNMs have good dispersion and magnetic separation properties.

Wide-angle XRD patterns (Figure 1(c)) show that the material is made up of inverse apical ferrite (Fe_3O_4) strucutre, confirmed by 2θ peaks at 30.1, 35.5, 43.1, 53.5, 57.0 and 62.7° that correspond to the crystal planes at (220), (331), (400), (422), (551) and (440) (Elmobarak & Almomani 2021). No other impurity peaks appear, indicating that the material is of high purity. The formation of amorphous SiO_2 is inferred from diffraction peak at 23°, indicating that the prepared material is SiO_2-coated Fe_3O_4. The XRD characteristic peaks of FNMs/APTES remain unchanged, indicating that the modified material does not destroy the crystal structure. As shown in Figure 1(d), the peak at 2.88° represents the characteristic peak of the hexagonal mesoporous silica, indicating that the prepared FNMs are hexagonal mesoporous structures and shows the regular arrangement. Compared with FNMs, the intensity of the diffraction peak of FNMs/APTES is significantly reduced. This is because the modifier APTES enters into the mesoporous pore, and the pore effect reduces the intensity of the diffraction peak.

The N_2 adsorption desorption isotherms and the pore size distribution of the materials are shown in Figure 1(e) and 1(f). It was illustrated that a rapid decrease of surface area was obtained after APTES modification on the FNMs (from 519.02 to 393.43 m^2·g^{-1}). FNMs are mesoporous materials with an average pore size of 2.26 nm and a pore volume of 0.30 cm^3·g^{-1} that reduced to 2.20 nm and 0.25 cm^3·g^{-1}, respectively, after APTES modification, which may be because of the entry of APTES into the mesoporous channel of FNMs.

The FT-IR spectrum of FNMs and FNMs/APTES are observed in Figure 2(a). Both samples show stretching vibration peak at 575 cm^{-1}, corresponding to the Fe–O of Fe_3O_4 (Elmobarak & Almomani 2021). The absorption bands in the ranges of 800 and 1,070 cm^{-1} are related to the symmetric and asymmetric stretching vibrations, respectively, of the siloxane (Si–O–Si) network structure. In contrast to FNMs, the FNMs/APTES band at 1,565 cm^{-1} was associated with the N–H groups bending vibrations in groups, and the characteristic peak of –CH_2 at 2,930 cm^{-1}, indicating that APTES has been successfully anchored on FNMs (Zhang *et al.* 2013).

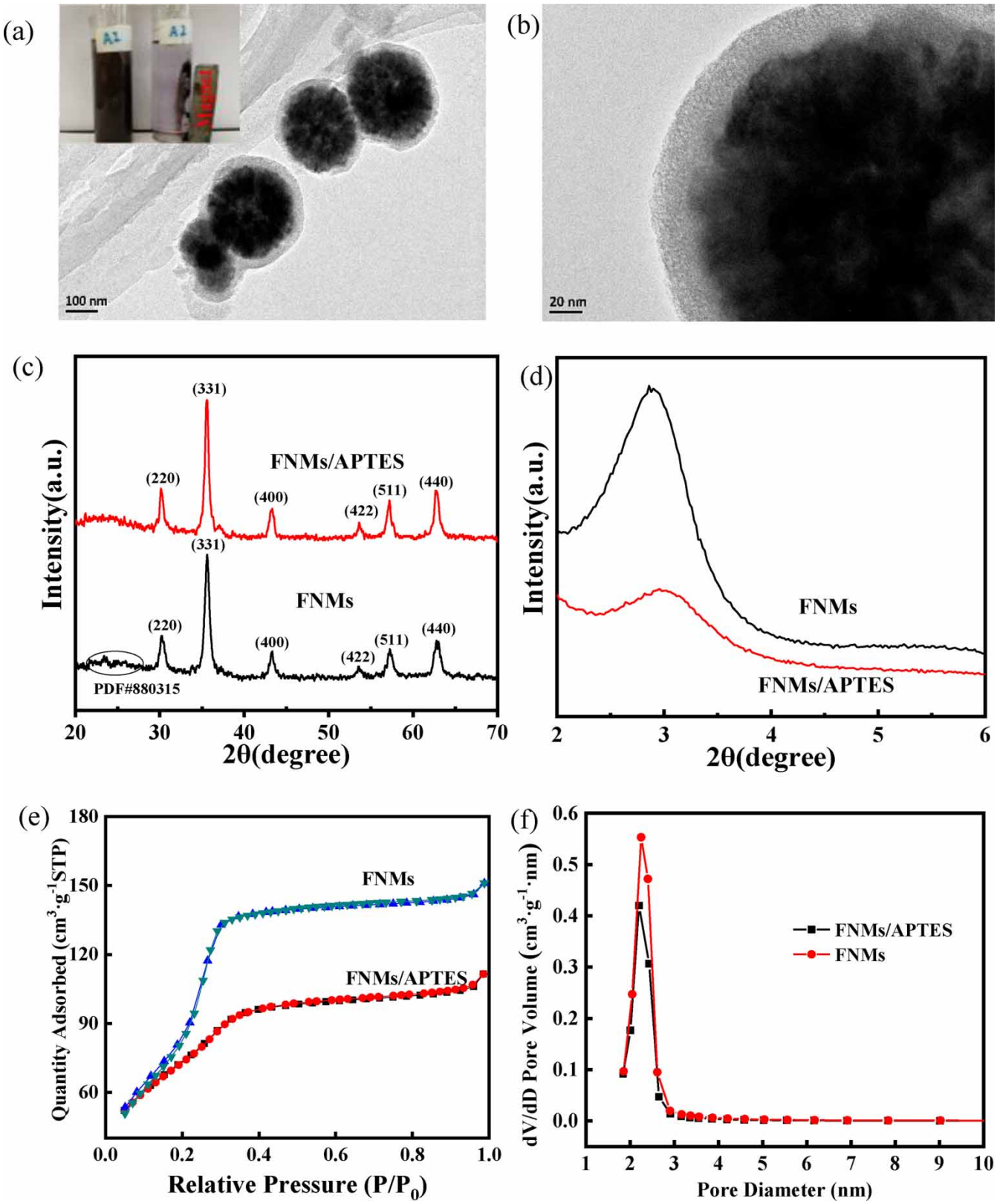

Figure 1 | TEM images of FNMs (a, b), wide-angle (c) and low-angle (d) XRD patterns, N_2 adsorption desorption isotherms (e), and the pore size distribution curves (f) of FNMs and FNMs/APTES.

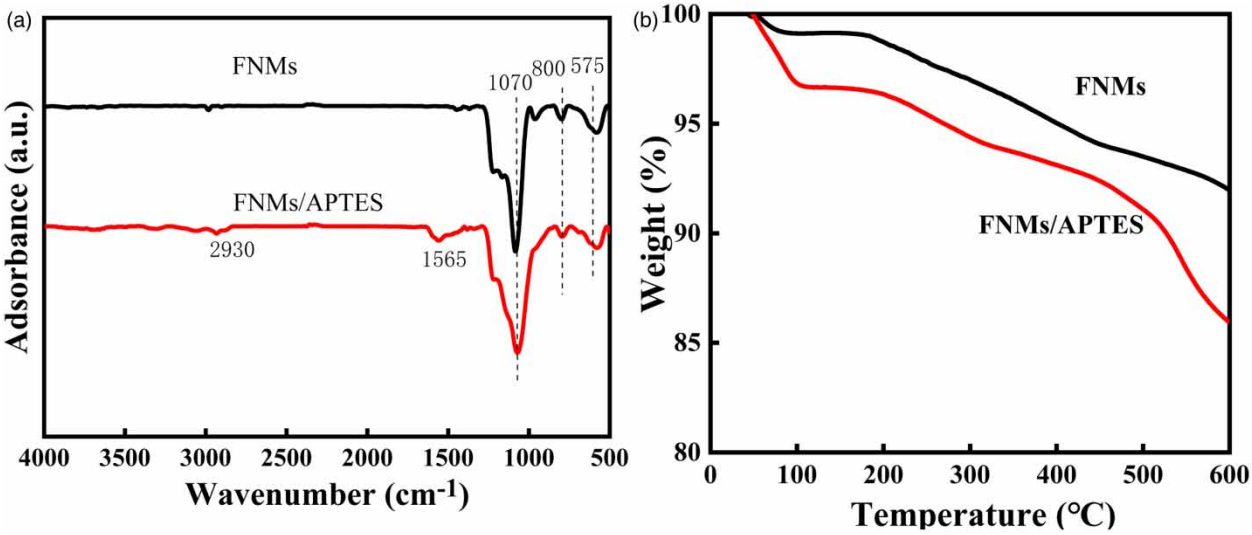

Figure 2 | The FT-IR spectrum (a) and TGA curves (b) of FNMs and FNMs/APTES.

Thermogravimetric (TGA) curve (Figure 2(b)) indicated the mass loss of FNMs and FNMs/APTES was 8 and 14.05% between 20 and 600 °C. The FNMs exhibited a weight loss below 200 °C, which was due to the loss of adsorbed water. The weight loss observed from 200 to 600 °C is due to the loss of structural water. For FNMs/APTES, the loss in mass below 200 °C is due to departure of adsorbed water molecules, while the weight loss from 200 to 600 °C resulted from the decomposition of the organic compounds anchored on FNMs. The TGA loss of FNMs (8%) was significantly lower than that of FNMs/APTES (14.05%), indicating the successful modification on the surface of FNMs with APTES.

The VSM analyses of FNMs and FNMs/APTES are shown in Figure 3. The magnetic hysteresis curves with no residual magnetization and coercivity in samples were observed, suggesting that the adsorbent was essentially superparamagnetic. The saturation magnetization of the FNM particles was measured to be 49.50 emu·g^{-1}. After modification with APTES, the magnetization was reduced to 42.70 emu·g^{-1}. The magnetism of FNMs/APTES is slightly lower than FNMs, depicting the successful location of NH_2 groups on the surface of FNMs.

3.2. Stability experiment

The stability test results of the material under acidic conditions are shown in Table 1. From the results, the dissolution rate of Fe increases with the increase of HCl concentration and immersion time. When the concentration of HCl was below 0.5 mol·L^{-1}, the dissolution rate was less than 0.5% when the immersion time was 60 h. The dissolution rate of FNMs

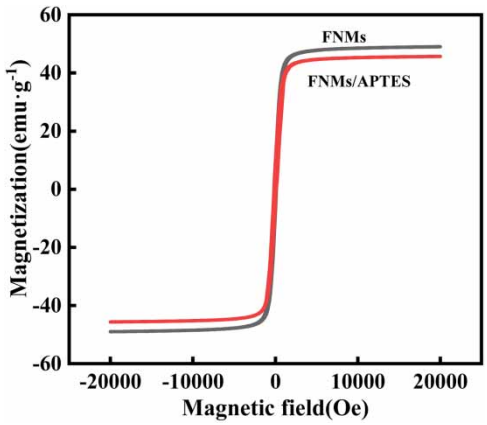

Figure 3 | The VSM of FNMs and FNMs/APTES.

Table 1 | Material stability of FNMs in HCl solution at different immersion times

HCl concentration (mol·L^{-1})	Leached Fe content (%)			
	24 h	36 h	48 h	60 h
0.05	0.05	0.07	0.17	0.24
0.1	0.07	0.08	0.20	0.27
0.5	0.17	0.20	0.32	0.46
1.0	1.11	1.82	5.33	6.19

increased significantly at HCl concentration of 1.0 mol·L^{-1}, and the dissolution rate is 6.19% after 60 h of immersion. Thus, the dissolution rate of Fe is low and FNMs demonstrated a good and stability under weak acid conditions.

3.3. Equilibrium studies

The adsorption of Cr(III)–EDTA with different concentrations onto three temperature conditions (15, 25 and 35 °C) was studied at pH 4.0. Compared with FNMs, FNMs/APTES shows the best adsorption amount of Cr(III)–EDTA, which is much larger than FNMs, indicating that amino groups of the adsorbent play the key role in Cr(III)–EDTA adsorption. As illustrated in Figure 4, as the concentration of Cr(III)–EDTA increases, the equilibrium adsorption capacity shows a trend of steep increase first and then a gentle increase. The maximum adsorption amount of Cr(III)–EDTA on the adsorbent at 15, 25 and 35 °C was 12.58, 13.13 and 14.00 mg·g^{-1}, respectively. Table 2 lists the calculated parameters calculated from Langmuir model and Freundlich model. From the result, the Freundlich model can fit the Cr(III)–EDTA adsorption on FNMs/APTES, reflecting that the adsorption process is multi-layer adsorption.

3.4. The influence of temperature

Table 3 shows that the thermodynamic parameters for Cr(III)–EDTA adsorption on FNMs/APTES were calculated from the Gibbs–Helmholtz equation. The $\Delta G°$ is a negative value and decreases with increasing temperature, indicating that the adsorption of Cr(III)–EDTA by FNMs/APTES is a spontaneous process. In combination with increasing adsorption (Figure 4), $\Delta H°$ and $\Delta S°$ are positive, demonstrating that the adsorption process is an endothermic reaction and increases the disorder of the solid–liquid system.

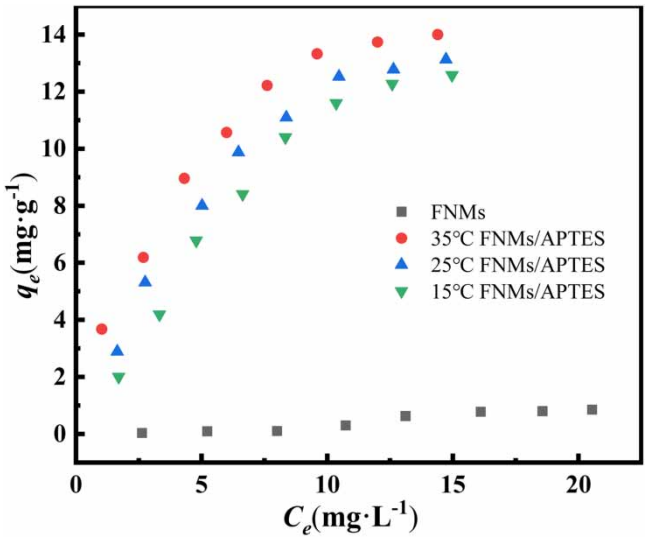

Figure 4 | Adsorption isotherms of Cr(III)–EDTA on FNMs/APTES and FNMs.

Table 2 | Isotherm parameters for Cr(III)–EDTA adsorption onto FNMs/APTES

	Langmuir			Freundlich		
Temperature (°C)	q_m (mg·g^{-1})	b (L·mg^{-1})	R^2	n	K_f (L·mg^{-1})	R^2
35	19.11	0.20	0.978	1.87	3.81	0.979
25	22.62	0.11	0.941	1.47	2.44	0.946
15	36.23	0.04	0.615	5.82	1.48	0.957

Table 3 | Thermodynamic parameters of Cr(III)–EDTA adsorption by FNMs/APTES

Temperature (°C)	$\Delta H°$ (kJ·mol^{-1})	$\Delta S°$ (J·mol^{-1}·K^{-1})	$\Delta G°$ (kJ·mol^{-1})
15	20.83	84.98	−3.66
25	20.83	84.98	−4.51
35	20.83	84.98	−5.36

3.5. Adsorption kinetics

The kinetic behavior of Cr(III)–EDTA adsorption by FNMs/APTES at an initial concentration of 15 mg·L^{-1} at 25 °C was investigated by fitting the kinetic data with the pesudo-first-order and peudo-second-order kinetic models (Figure 5). As shown in Figure 2, the maximum adsorption capacity of Cr(III)–EDTA increases with the increase of contact time (2–60 min), and the maximum adsorption capacity of Cr(III)–EDTA tends to be constant after 200 min. The kinetic constants calculated from the model fitting are shown in Table 4. The correlation coefficient (R^2) calculated from pseudo-second-order kinetics was greater than that of pseudo-first-order kinetics, and the calculated adsorption amount was similar to the actual adsorption capacity, indicating that pseudo-second-order kinetics equation could better fit the adsorption of Cr(III)–EDTA by FNMs/APTES and Cr(III)–EDTA adsorption on the adsorbent was a chemical process.

3.6. Effect of pH on Cr(III)–EDTA adsorption

The effect of pH on the adsorption of Cr(III)–EDTA onto FNMs/APTES is presented in Figure 6(a). It was clear that the adsorption capacity of Cr(III)–EDTA increases in the pH range of 2.0–4.0, whereas a dramatic decrease occurred at pH above 5.0, and high adsorption was observed at pH 4.0–5.0. At low pH, Cr(III)–EDTA mainly exists in the form of

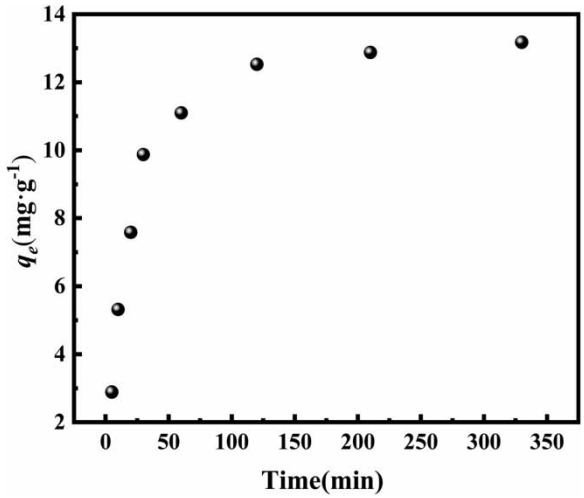

Figure 5 | Effect of contact time on Cr(III)–EDTA adsorption onto FNMs/APTES.

Table 4 | Fitting parameters of pseudo-first-order and pseudo-second-order kinetic equations of Cr(III)–EDTA adsorbed on FNMs/APTES

		Pseudo-first-order			Pseudo-second-order		
C_0 (mg·L^{-1})	q_e (mg·g^{-1})	$K1$[g·(mg·min^{-1})]	q_{cal}(mg·g^{-1})	R^2	$K2$[g·(mg·min^{-1})]	q_{cal}(mg·g^{-1})	R^2
12	13.18	6.55×10^{-3}	2.311	0.956	4.79×10^{-3}	13.781	0.999

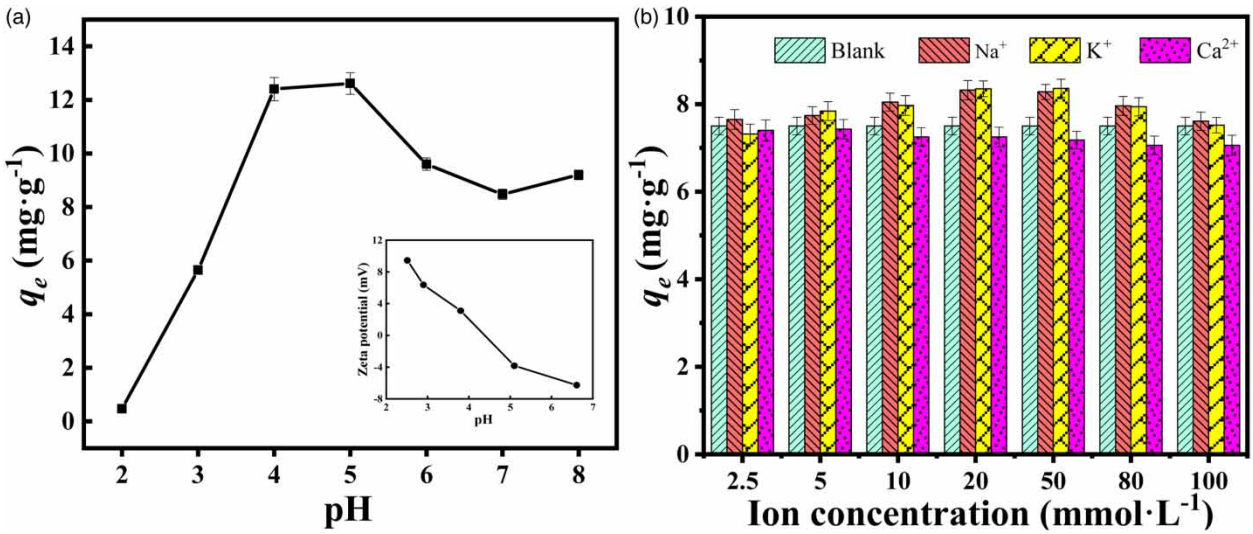

Figure 6 | Effect of pH (a) and coexisting ions (b) on the adsorption of Cr(III)–EDTA by FNMs/APTES.

[Cr–EDTA]$^-$, [Cr-H–EDTA](aq), [Cr–OHEDTA]$^{2-}$ anions and molecules in the solution (Cao *et al.* 2011), while the amino groups of FNMs/APTES are easy to be protonated under acidic conditions. It can see from the illustration in Figure 7(a), the isoelectric point of FNMs/APTES is pH 4.4, and the amino groups on the adsorbent are in a protonated state at pH $<$ 4.4, and the Cr(III)–EDTA anions are combined with the protonated amino groups of the adsorbents and removed by electrostatic interaction. When pH was $>$3.0, the content of [Cr–EDTA]$^-$ in the solution began to decline, whereas the content of [Cr–OHEDTA]$^{2-}$ increased, and the electrostatic attraction interaction between Cr(III)–EDTA anions and the protonated amino groups of the adsorbents was enhanced, leading to augmented Cr(III)–EDTA adsorption. However, when the pH was $>$5, the adsorption capacity decreases gradually with the further increase of solution pH, which may be related to the electrostatic repulsion interaction between Cr(III)–EDTA anions and negatively charged adsorbents in the solution.

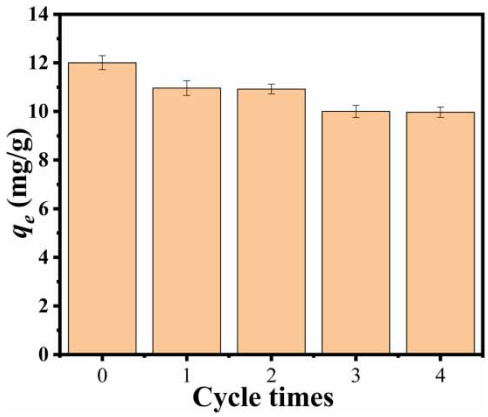

Figure 7 | Adsorption of Cr(III)–EDTA by FNMs/APTES and regenerated adsorbent.

Experimental results show that the pH of the adsorbed solution tended to be neutral. H^+ in the solution participates in the protonation of amino groups on the adsorbent surface, which leads to the increase of pH of the solution in acidic condition. Under alkaline conditions, the pH decreases after the reaction may be due to OH^- in the water.

3.7. Effects of coexisting cation on adsorption

The effects of inorganic cations (Na^+, K^+, Ca^{2+}) may interfere in the adsorption of Cr(III)–EDTA onto the FNMs/APTES (Figure 6(b)). The results suggested that Na^+ and K^+ had some promoting effects on adsorption, whereas Ca^{2+} had inhibiting effects on adsorption. This is due to the addition of cations competing with the Cr(III)–EDTA in the solution for the adsorption site of the adsorbent. The addition of cations will compete with Cr(III)–EDTA for the adsorption site of the adsorbent. In the solution, due to the incomplete complexation between EDTA and Cr(III), the complexation ability of K^+, Ca^{2+} and Na^+ with EDTA is different. The order of the complex stability constants is: $K_{Cr-EDTA} = 23.4 > K_{Ca-EDTA} = 10.69 > K_{Na-EDTA} = 1.6 > K_{K-EDTA} = 0.8$. Therefore, Ca^{2+} is more likely to complex with EDTA in the solution, and result in the slightly reduced Cr(III)–EDTA adsorption on the adsorbent.

3.8. Reusability

The reusability experiments of FNMs/APTES were carried out by HCl solution and repeated for four adsorption–desorption cycles (Figure 7). The initial adsorption capacity was 12.01 $mg \cdot g^{-1}$, and after four adsorption–desorption experiments, the adsorption capacity of FNMs/APTES was 9.97 $mg \cdot g^{-1}$ (83.03% of the original adsorption amount). The decrease in Cr(III) adsorption is probably because of the incomplete desorption. The reusability of FNMs/APTES reflects that FNMs/APTES can be used as a promising candidate for Cr(III)–EDTA adsorption in water.

3.9. Adsorption mechanism

To describe the adsorption mechanism of FNMs/APTES, the adsorbents before and after adsorption of EDTA and Cr(III)–EDTA were analyzed by XPS. As shown in Figure 8(a) and Table 5, the peak of the spectral line at Si_{2P} of 102.38 eV before and after Cr(III)–EDTA adsorption indicated that the material surface is covered by an amorphous SiO_2 layer. XPS failed to detect Fe peaks, possibly due to the coating of the SiO_2 layer, which makes X-rays impenetrable. The characteristic peak of N 1 s at 399.39 eV indicated that the modification of amino groups was successful. After EDTA adsorption, the diffraction peak area of O increases from 46.14 to 47.12%, while N content decreases from 8.08 to 7.75, which indicates that EDTA has been

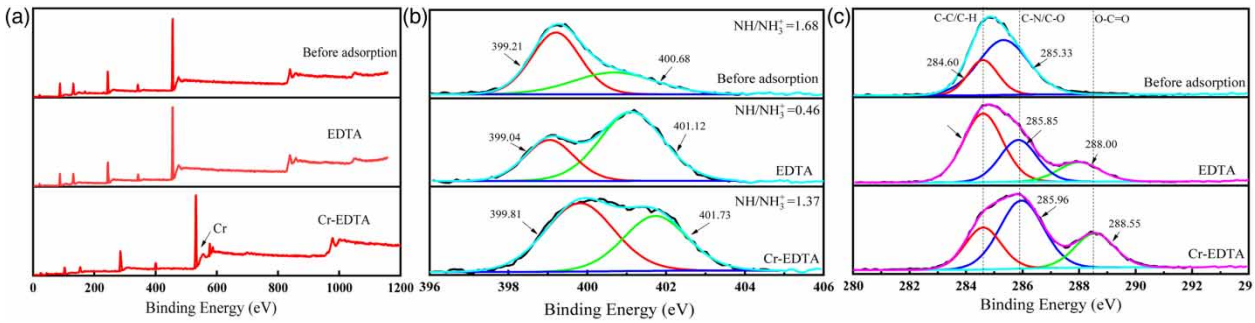

Figure 8 | XPS full spectrum (a), N 1 s spectrum (b), and C 1 s spectrum (c) of FNMs/APTES before and after EDTA and Cr(III)–EDTA adsorption.

Table 5 | Element content analysis of FNMs/APTES before and after EDTA and Cr–EDTA adsorption

Adsorbent	C	N	O	Cr
FNMs/APTES	45.36	8.08	46.14	–
FNMs/APTES after EDTA adsorption	44.93	7.75	47.12	–
FNMs/APTES after Cr–EDTA adsorption	45.92	7.13	45.46	1.48

anchored on the surface of the adsorbent. After Cr(III)–EDTA adsorption, the peaks of Cr 2P appeared, and N content of the adsorbent decreases, indicating that Cr(III)–EDTA chelates as a whole was anchored on the surface of FNMs/APTES.

The XPS spectra of N 1 s before and after Cr(III)–EDTA adsorption is observed in Figure 8(b). The characteristic peaks of the pre-adsorption amino group (–NH_2) and protonated amino group (–NH_3^+) appeared at 399.19 and 400.32 eV. After EDTA adsorption, the percentage of protonated amino groups on the adsorbent increased, which may be ascribed to the electrostatic interaction between EDTA anions in the solution and the protonated amino groups of the adsorbents. For Cr(III)–EDTA on FNMs/APTES, the ratio of protonated amino groups on FNMs/APTES decreased, which may be due to the electrostatic interaction between $[Cr–EDTA]^-$ and $[Cr–OHEDTA]^{2-}$ anions and protonated amino groups of the adsorbent. Moreover, the diffraction peaks of amino and protonated amino groups shifted toward the direction of high binding energy, which may be due to the formation of Cr(III)–amide complex compounds between Cr(III) and –NH_2 on the surface of FNMs/APTES (Wu *et al.* 2020).

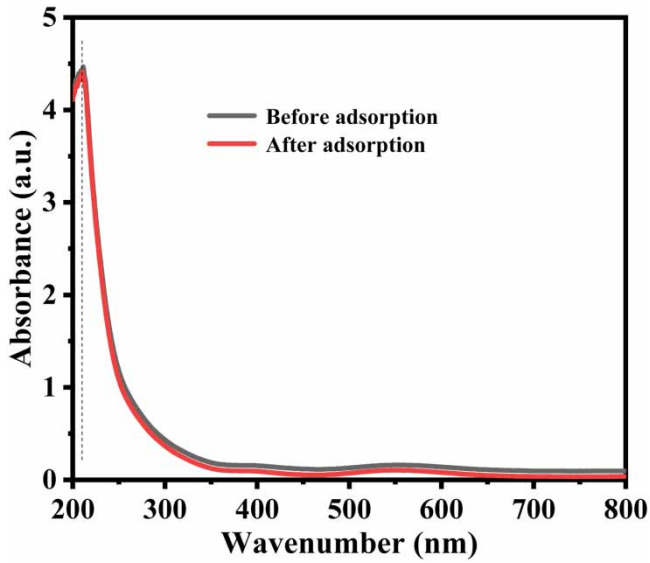

Figure 9 | UV–Vis NIR spectrum of Cr(III)–EDTA before and after adsorption.

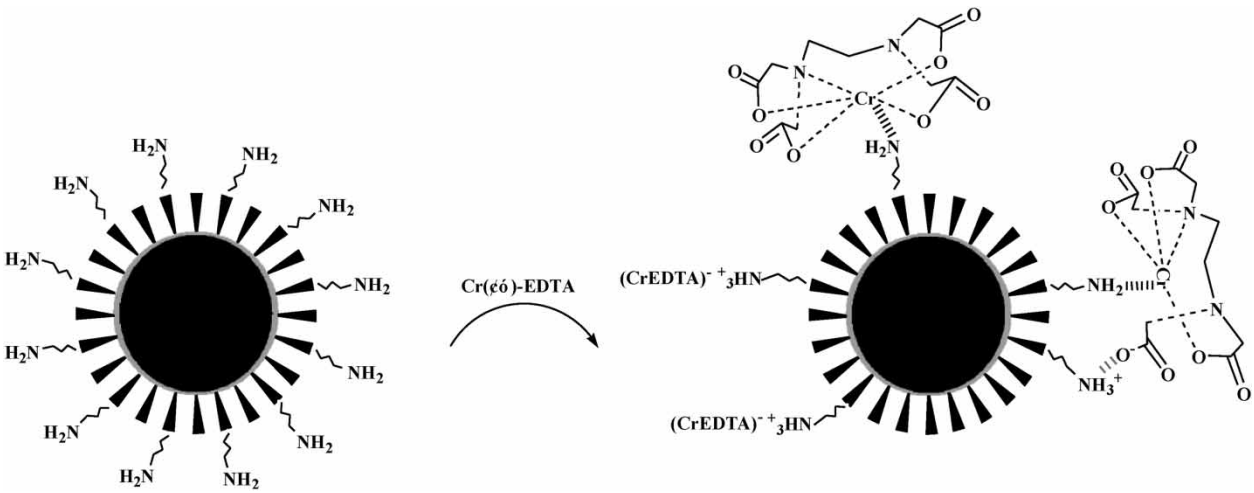

Figure 10 | Adsorption mechanism of Cr(III)–EDTA on FNMs/APTES.

The C 1 s XPS spectrum of FNMs/APTES before and after Cr(III)–EDTA adsorption are shown in Figure 8(c). The diffraction peaks of the FNMs/APTES at 284.60 and 285.96 eV correspond to the characteristic peaks of C–C and C–O, respectively. The C 1 s peak of FNMs/APTES before Cr(III) adsorption indicates the successful modification of FNMs by a silane coupling agent (APTES). After the adsorption of EDTA and Cr(III)–EDTA, the characteristic peaks of O–C = O of FNMs/APTES appeared, which may be due to the introduction of O–C = O in EDTA suggesting that Cr(III)–EDTA adsorption on the adsorbent was in the form of Cr(III)–EDTA. Before and after adsorption of Cr(III)–EDTA on FNMs/APTES, the Cr(III)–EDTA solution was subjected to UV–Vis NIR, and the results are shown in Figure 9. Cr(III)–EDTA solution peaked at 214 nm before and after Cr(III) adsorption without any changes, indicating that the Cr(III) adsorption did not change the morphology of Cr(III)–EDTA, and Cr(III)–EDTA chelate as a whole was adsorbed on the surface of the adsorbent.

Overall, the possible adsorption mechanism of Cr(III)–EDTA adsorption on FNMs/APTES is illustrated in Figure 10. Cr(III)–EDTA chelate exists mostly in the form of $[Cr–EDTA]^-$, [Cr-HEDTA] (aq), $[Cr–OHEDTA]^{2-}$ in water, and the amino groups on the adsorbent surface exist in the form of amino group and protonated amino group under acidic conditions. Cr(III)–EDTA chelate was removed as a whole by the electrostatic interaction between the $[Cr–EDTA]^-$, $[Cr–OHEDTA]^{2-}$ anions and the protonated amino groups of FNMs/APTES, and complexing action between the Cr(III) ions in Cr(III)–EDTA and amino groups of the adsorbent was another adsorption mechanism for Cr–EDTA adsorption.

4. CONCLUSIONS

In this work, FNMs/APTES was synthesized and used for the removal of Cr(III)–EDTA in water. The prepared FNMs/APTES exhibited good chemical stability for acid resistance. FNMs/APTES has a high adsorption capacity for Cr(III)–EDTA in water (13.13 $mg \cdot g^{-1}$) and has a good recycling performance. The XPS analysis confirmed that FNMs/APTEs showed significant differences before and after Cr(III)–EDTA adsorption. In addition, the presence of cations Na^+, K^+ and Ca^{2+} had a slight effect on adsorption, reflecting the potential application for heavy metal-organic chelate in high-salinity water. Cr(III)–EDTA in water was removed as a whole by FNMs/APTES through electrostatic attraction between Cr(III)–EDTA anions and the protonated amino groups of FNMs/APTES.

ACKNOWLEDGEMENT

We are thankful for the financial support provided by the National Natural Science Foundation of China (22076111), China.

DATA AVAILABILITY STATEMENT

All relevant data are included in the paper or its Supplementary Information.

CONFLICT OF INTEREST

The authors declare there is no conflict.

REFERENCES

Cao, X. H., Guo, J., Mao, J. & Lan, Y. L. 2011 Adsorption and mobility of Cr(III)-organic acid complexes in soils. *J. Hazard. Mater.* **192** (3), 1533–1538.

Chen, N. Y. & Pan, B. C. 2020 A preliminary exploration on Au nanoparticles-mediated colorimetric analysis of Cr(III)-carboxyl complexes in synthetic and authentic water samples. *Chem. Eng. J.* **387**, 124079.

Cheng, Y., Xiao, Z., Yu, H., Wan, M. & Mang, L. 2017 Preparation and adsorption properties of amino modified mesoporous microsphere Fe_3O_4@SiO_2@$msio_2$ magnetic adsorbent. *J. Funct. Mater.* **48** (12), 12135–12141.

Durante, C., Cuscov, M., Isse, A. A., Sandona, G. & Gennaro, A. 2011 Advanced oxidation processes coupled with electrocoagulation for the exhaustive abatement of Cr-EDTA. *Water Res.* **45**, 2122–2130.

Egodawatte, S., Datt, A., Burns, E. A. & Larsen, S. C. 2015 Chemical insight into the adsorption of chromium(III) on iron oxide/mesoporous silica nanocomposites. *Langmuir* **31** (27), 53–62.

Elmobarak, W. F. & Almomani, F. 2021 Application of Fe_3O_4 magnetite nanoparticles grafted in silica (SiO_2) for oil recovery from oil in water emulsions. *Chemosphere* **265**, 129054.

Eyvazi, B., Jamshidi-Zanjani, A. & Darban, A. K. 2019 Synthesis of nano-magnetic $mnfe_2o_4$ to remove Cr(III) and Cr(VI) from aqueous solution: a comprehensive study. *Environ. Pollut.* **265**, 113685.

Guan, X., Chen, Y. & Fan, H. 2017 Stepwise deprotonation of magnetite-supported gallic acid modulates oxidation state and adsorption-assisted translocation of hexavalent chromium. *ACS Appl. Mater. Interfaces* **155**, 1–8.

Guimaraes, T. G., Paquini, L. D., Lyrio Ferraz, B. R., Roberto Profeti, L. P. & Profeti, D. 2020 Efficient removal of Cu(II) and Cr(III) contaminants from aqueous solutions using marble waste powder. *J. Environ. Chem. Eng.* **8**, 103972.

Hai, J., Liu, L. & Tan, W. 2020 Catalytic oxidation and adsorption of Cr(III) on iron-manganese nodules under oxic conditions. *J. Hazard Mater.* **390**, 122166.

Hao, X., Tao, E., Yang, S. Y. & Li, Y. 2021 A new montmorillonite-based porous composites: effectively removal of Cr(III)-organic complexes in tannery wastewater. *J. Polym. Environ.* **30**, 308–318.

Liu, W. Y. 2021 Removal of recalcitrant trivalent chromium complexes from industrial wastewater under strict discharge standards. *Environ. Technol. Innov.* **23**, 101644.

Lofrano, G., Meric, S., Zengin, G. E. & Orhon, D. 2013 Chemical and biological treatment technologies for leather tannery chemicals and wastewaters: a review. *Sci. Total Environ.* **461**, 265–281.

Luther, S., Brogfeld, N., Kim, J. & Parsons, J. G. 2013 Study of the thermodynamics of chromium(III) and chromium(VI) binding to iron(II/III) oxide or magnetite or ferrite and magnanese(II) iron (III) oxide or jacobsite or manganese ferrite nanoparticles. *J. Colloid Interface Sci.* **400** (12), 97–103.

Novotnik, B., Scancar, J., Milacic, R., Filipic, M. & Zeura, B. 2016 Cytotoxic and genotoxic potential of Cr(VI), Cr(III)-nitrate and Cr(III)-EDTA complex in human hepatoma (hepg2) cells. *Chemosphere* **154**, 124–131.

Su, H., Fang, Z., Fang, Z. Q., Tsang, P. E., Fang, J. Z. & Zhao, D. Y. 2016 Stabilisation of nanoscale zero-valent iron with biochar for enhanced transport and in-situ remediation of hexavalent chromium in soil. *Environ. Pollut.* **214**, 94–100.

Tang, Y. L., Zhao, J. T., Zhou, J. F., Zeng, Y. H., Zhang, W. H. & Shi, B. 2020 Highly efficient removal of Cr(III)-poly(acrylic acid) complex by coprecipitation with polyvalent metal ions: performance, mechanism, and validation. *Water Res.* **178**, 115807.

Wang, P., Du, S., Zhang, S. N., Huang, X. & Huang, F. 2019 Constructing mesoporous phosphated titanium oxide for efficient Cr(III) removal. *J. Hazard. Mater.* **384**, 121278.

Wang, J. H., Atif, S. & Zhang, D. 2020a Adsorption of Cr(III) by EGTA modified magnetic microsphere: effect of high salinity and organic chelating acids. *Environ. Technol. Innovat.* **20**, 101088.

Wang, J. H., Mao, M., Atif, S. & Chen, Y. 2020b Adsorption behavior and mechanism of aqueous Cr(III) and Cr(III)-EDTA chelates on DTPA-chitosan modified Fe_3O_4@SiO_2. *React. Funct. Polym.* **156**, 104720.

Wang, J. H., Tong, X. H. & Chen, Y. 2020c Enhanced removal of Cr(III) in high salt organic wastewater by EDTA modified magnetic mesoporous silica. *Micropor. Mesopor. Mater.* **303**, 110262.

Wang, J. H., Chen, Y., Sun, T. T., Liang, L. L. & Wang, C. 2021 Enhanced removal of Cr(III)-EDTA chelates from high-salinity water by ternary complex formation on DETA functionalized magnetic carbon-based adsorbents. *Ecotoxicol. Environ. Saf.* **209**, 111858.

Wu, H. M., Xiao, Y., Guo, Y., Miao, S. J., Chen, Q. Q. & Chen, Z. 2020 Functionalization of SBA-15 mesoporous materials with 2-acetylthiophene for adsorption of Cr(III) ions. *Micropor. Mesopor. Mater.* **292**, 109754.

Xu, Z., Zhang, Q. R., Li, X. C. & Huang, X. F. 2022 A critical review on chemical analysis of heavy metal complexes in water/wastewater and the mechanism of treatment methods. *Chem. Eng. J.* **429**, 131688.

Ye, Y., Shan, C., Zhang, X., Liu, H., Wang, D., Lv, L. & Pan, B. 2018 Water decontamination from Cr(III)-organic complexes based on pyrite/H_2O_2: performance, mechanism, and validation. *Environ. Sci. Technol.* **52**, 10657–10664.

Zhang, J., Zhai, S., Li, S., Xiao, Z. Y., Song, Y., An, Q. D. & Tian, G. 2013 Pb(II) removal of Fe_3O_4@SiO_2-NH_2 core-shell nanomaterials prepared via a controllable sol-gel process. *Chem. Eng. J.* **215**, 461–471.

Zhang, Y. H., Xu, X. M., Yue, C. L., Song, L., Lv, Y. Z., Liu, F. Q. & Li, A. M. 2021 Insight into the efficient co-removal of Cr(VI) and Cr(III) by positively charged UiO-66-NH_2 decorated ultrafiltration membrane. *Chem. Eng. J.* **404**, 126546.

Zhang, W., Li, Q., Li, R., Shen, N., Li, J. S., Shen, J. Y., Sun, X. Y. & Han, W. Q. 2022 Enhanced sequestration of chelated Cr(III) from aqueous by Al-containing ferrihydrite: new expectation of overall removal of various heavy metal complexes. *Sep. Purif. Technol.* **282**, 120151.

First received 8 September 2022; accepted in revised form 8 January 2023. Available online 20 January 2023